

Effects of spin–orbit coupling on the coupled $3^3\Pi$ and $4^3\Pi$ excited states of NaK

A.D. Wilkins¹, L. Morgus², J. Huennekens, A.P. Hickman*

Department of Physics, Lehigh University, 16 Memorial Dr. East, Bethlehem, PA 18015, USA

ARTICLE INFO

Article history:

Received 2 August 2009

In revised form 21 August 2009

Available online 27 August 2009

Keywords:

Fine structure

Avoided crossing

NaK

Excited states

ABSTRACT

Spin–orbit coupling constants calculated for several excited states of the NaK molecule are used to interpret recent experiments. The theoretical results, which provide coupling constants as a function of internuclear separation R , were convoluted with vibrational wavefunctions in order to determine vibrational-state-dependent spectroscopic constants that could be compared with recent measurements for the $3^3\Pi$ state. Sharp structure in the experimental data could be attributed to rapid changes in the adiabatic spin–orbit coupling near an avoided crossing.

© 2009 Elsevier Inc. All rights reserved.

1. Introduction

Several recent high-resolution spectroscopic studies in our laboratory have probed the fine and hyperfine structure of various excited triplet states of the NaK molecule [1–6]. Other studies have addressed singlet–triplet spin–orbit coupling [3,7–9]. These studies have determined the fine structure coupling constants for many different vibrational levels of several electronic states. In the present paper we address the unusual behavior observed for the $3^3\Pi$ state [4]. Our analysis is based on our *ab initio* calculations of the fine structure coupling constants as a function of the internuclear separation R performed with the GAMESS electronic structure code [10].

The present work complements our previous experimental and theoretical studies of the coupled $3^3\Pi$ and $4^3\Pi$ electronic states. These states exhibit an avoided crossing, leading to a double well in the $3^3\Pi$ state. Previous studies [4,6] measured the rovibrational energy levels of the $3^3\Pi$ state and accurately determined the double well shape of that electronic potential. Morgus et al. [4] noticed unusual oscillatory structure in the dependence of the rotational constants B_v on the vibrational quantum number v that could be explained by the double well. Here we investigate the effects of the double well and the avoided crossing on fine structure coupling constants A_v , which have been measured [4] for many different vibrational levels of the $3^3\Pi$ and estimated [11] for a few levels of the $4^3\Pi$ state. The dependence of A_v on v exhibits anomalous struc-

ture, which we can calculate by convoluting a theoretical coupling function $A(R)$ with the square of the vibrational wavefunctions $\chi_v(R)$. The sharp change in the form of $A(R)$ near the avoided crossing and the nature of the vibrational wavefunctions $\chi_v(R)$ in the double well lead to the anomalous behavior of A_v . By drawing on our previous experimental work for the most accurate potential curves and vibrational wavefunctions and combining these with the present theoretical calculations of spin–orbit coupling functions, we achieve very satisfactory agreement with the values of A_v measured for the $3^3\Pi$ state.

Several excited state potential curves of NaK are shown in Fig. 1. The adiabatic $3^3\Pi$ and $4^3\Pi$ states we address in the present work are highlighted. The calculations also included all adiabatic states correlating to the $3s4s$, $3s4p$, $3p4s$, $3s5s$, $3s3d$, $3s5p$, and $4s4s$ separated atom limits. We show the curves calculated by Magnier et al. [12], which include adjustments based on experimental atomic data and therefore provide an excellent overall picture.

This paper is organized as follows: Section 2 briefly describes the theoretical calculations that have been performed. The main results are presented and discussed in Section 3, and Section 4 contains concluding remarks.

2. Theory

2.1. Methodology implemented in GAMESS

We used the GAMESS electronic structure code [10] to calculate electronic wavefunctions and spin–orbit coupling matrix elements for several excited states of NaK. Optimized orbitals were calculated at the multi-configuration self-consistent field (MCSCF) level. The active space included $\text{Na}(3s, 3p, 4s)$ and $\text{K}(4s, 4p, 5s, 3d, 5p)$ orbitals. The MCSCF orbitals were then used to calculate the singlet

* Corresponding author. Fax: +1 610 758 5730.

E-mail addresses: jph7@lehigh.edu (J. Huennekens), aph2@lehigh.edu (A.P. Hickman).

¹ Present address: Department of Molecular and Human Genetics, Baylor College of Medicine, Houston, TX 77030, USA.

² Present address: Thorlabs, Inc., Newton, NJ 07860, USA.

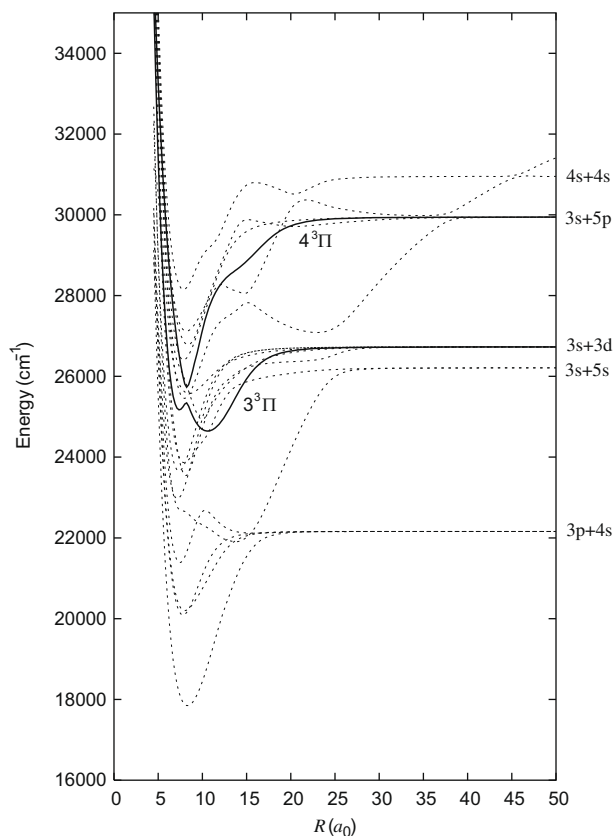


Fig. 1. Electronic potential curves for high lying triplet and singlet states of NaK calculated by Magnier et al. [12]. The solid curves represent the states investigated in this work.

and triplet electronic wavefunctions using a full configuration interaction (CI) for the two valence electrons in a space of 86 orbitals. The basis set was Dunning's triple-zeta valence (TZV) [13], augmented to include long range orbitals [6] for a better description of excited states. The added orbitals are listed in Table 1.

Electronic wavefunctions Ψ_i were calculated for several electronic states. The functions Ψ_i , which are defined in *LS* coupling, are then used to calculate matrix elements of the spin-orbit Hamiltonian \mathbf{H}_{so} . The form of \mathbf{H}_{so} implemented in GAMESS is obtained by starting with the full Breit–Pauli spin-orbit Hamiltonian and then replacing the two-electron part with a one-electron approximation [14]. The final expression is

$$\mathbf{H}_{so} = \frac{\alpha^2}{2} \sum_i \sum_K \frac{Z_{\text{eff},K}}{r_{iK}^3} \mathbf{l}_{iK} \cdot \mathbf{s}_i, \quad (1)$$

where α is the fine structure constant, and \mathbf{l} and \mathbf{s} denote electron orbital and spin angular momenta, respectively. The nuclei are de-

noted by K and the electrons by i . GAMESS permits using effective nuclear charges Z_{eff} , but we chose to use the full nuclear charge. The matrix elements of the full Hamiltonian may be written

$$H_{ij} = \langle \Psi_i | (\mathbf{H}_{\text{elec}} + \mathbf{H}_{so}) | \Psi_j \rangle = \delta_{ij} E_i + \langle \Psi_i | \mathbf{H}_{so} | \Psi_j \rangle. \quad (2)$$

This matrix is then diagonalized to obtain the energy levels, including fine structure, as a function of internuclear separation R .

2.2. Extensions to GAMESS' methodology

The methodology implemented in GAMESS is designed to calculate energy levels. Because our objective was to calculate coupling terms explicitly, we made several adjustments in the procedure described above. For example, the electronic states Ψ_i are formulated using real angular functions, so that the well-defined quantum numbers include Σ and Λ , the projections of the spin and orbital electronic angular momenta, respectively, on the internuclear axis. No explicit account is taken of the Ω quantum number in GAMESS. The diagonalization of $\mathbf{H}_{\text{elec}} + \mathbf{H}_{so}$ at various values of R still leads exactly to the desired energies. However, the present application involves disentangling a large number of excited states, and it was advantageous to block diagonalize the matrix $\mathbf{H}_{\text{elec}} + \mathbf{H}_{so}$ by transforming to a basis that explicitly depended on Ω . The matrix $\mathbf{H}_{\text{elec}} + \mathbf{H}_{so}$ was intercepted and written to a file before it was diagonalized. Then a second computer code implemented a transformation to a basis depending on Ω and completed the calculation.

The electronic wavefunctions we calculated using GAMESS are made up of the spatial atomic orbitals $s, p_x, p_y, p_z, d_{z^2}, d_{xz}, d_{yz}, d_{xy}$, and $d_{x^2-y^2}$. These states are multiplied by electron spin states $|\Sigma\rangle$ (the Σ in the ket $|\Sigma\rangle$ represents the projection of the electron spin S on the internuclear axis, and should not be confused with the Σ^+ that identifies electronic states with $\Lambda = 0$). The spatial orbitals can be expressed as spherical harmonics, and the product states of spherical harmonics and spin orbitals corresponding to specific values of Ω can also be written explicitly. Working out the details allows the necessary transformation to be determined. For those states that dissociate to an s atom and a p atom, the possible electronic states can be denoted by $^1\Sigma^+, ^3\Sigma^+, ^1\Pi_x, ^3\Pi_x, ^1\Pi_y$, and $^3\Pi_y$, where a subscript x or y signifies an electronic wavefunction built, respectively, from real p_x or p_y orbitals formed from linear combinations of spherical harmonics. The addition of the electron spin allows us to identify $\Omega (= \Lambda + \Sigma)$, and we give the value of Ω as a subscript. The wavefunctions for the four Σ^+ states can then be written

$$\begin{aligned} |\Sigma^+\rangle|00\rangle &= |^1\Sigma_0^+\rangle \\ |\Sigma^+\rangle|1,-1\rangle &= |^3\Sigma_{-1}^+\rangle \\ |\Sigma^+\rangle|10\rangle &= |^3\Sigma_0^+\rangle \\ |\Sigma^+\rangle|11\rangle &= |^3\Sigma_1^+\rangle. \end{aligned} \quad (3)$$

The wavefunctions for the four Π_x states are

$$\begin{aligned} |\Pi_x\rangle|00\rangle &= \frac{1}{\sqrt{2}} [|^1\Pi_1\rangle - |^1\Pi_{-1}\rangle] \\ |\Pi_x\rangle|1,-1\rangle &= \frac{1}{\sqrt{2}} [|^3\Pi_0\rangle - |^3\Pi_{-2}\rangle] \\ |\Pi_x\rangle|10\rangle &= \frac{1}{\sqrt{2}} [|^3\Pi_1\rangle - |^3\Pi_{-1}\rangle] \\ |\Pi_x\rangle|11\rangle &= \frac{1}{\sqrt{2}} [|^3\Pi_2\rangle - |^3\Pi_0\rangle]. \end{aligned} \quad (4)$$

The wavefunctions for the four Π_y states are

Table 1
The long range s, p , and d gaussian basis functions used to augment the TZV basis set [6,13].

Na	Exponent	K	Exponent
s	0.007660	s	0.006000
		p	0.063900
		p	0.019800
		p	0.005200
d	0.271900	d	0.173200
		d	0.090640
		d	0.028900
		d	0.010000

$$\begin{aligned}
|\Pi_y\rangle|00\rangle &= \frac{1}{\sqrt{2}} [|^1\Pi_1\rangle + |^1\Pi_{-1}\rangle] \\
|\Pi_y\rangle|1, -1\rangle &= \frac{1}{\sqrt{2}} [|^3\Pi_0\rangle + |^3\Pi_{-2}\rangle] \\
|\Pi_y\rangle|10\rangle &= \frac{1}{\sqrt{2}} [|^3\Pi_1\rangle + |^3\Pi_{-1}\rangle] \\
|\Pi_y\rangle|11\rangle &= \frac{1}{\sqrt{2}} [|^3\Pi_2\rangle + |^3\Pi_0\rangle]. \quad (5)
\end{aligned}$$

Now that we have a relationship between the GAMESS basis and the basis needed for the sp case, we can write a 12×12 transformation matrix for electronic states. The transformation separates the states according to the Ω quantum number and facilitates the analysis of the results of the sp case.

The molecular states that can be constructed from an s atom and a p atom are $^1\Sigma^+$, $^3\Sigma^+$, $^1\Pi$, and $^3\Pi$. In the separated atom limit, the spin-orbit interaction depends on only one constant, which we denote A^{sp} , and which may be identified with the constant A in the effective spin-orbit operator $AL \cdot S$ for the p atom. However, as the atoms approach each other, different interactions are possible between the different states. The three equivalent p orbitals of the separated atoms are transformed into a p_z orbital oriented parallel to the molecular axis and two equivalent perpendicular orbitals (p_x and p_y). The orbitals also depend on whether the molecular state is a singlet or triplet. In all, there are five distinct “spin-orbit constants” that define the possible matrix elements of \mathbf{H}_{so} between the molecular states that arise in the sp case. We denote these constants $A_1^{sp} - A_5^{sp}$, and we relate them to the coupling between specific molecular states in Table 2. At large internuclear distance R , A_1^{sp} through A_5^{sp} will all approach A_{sp} , which is 1/3 of the calculated spin-orbit splitting of the separated atom 2P state.

Similarly the molecular states that can be constructed from an s atom and a d atom are $^1\Sigma^+$, $^3\Sigma^+$, $^1\Pi$, $^3\Pi$, $^1\Delta$, and $^3\Delta$. As in the sp case, the spin-orbit interaction at the separated atom limit depends on one constant, A^{sd} , which depends only on the electron in the d orbital. In the molecular picture, there are five d orbitals: d_{z^2} , d_{xz} , d_{yz} , d_{xy} , and $d_{x^2-y^2}$. The first three of these correspond to Σ^+ and Π states, and the transformation relating the GAMESS basis to the basis in which Ω is a good quantum number is equivalent to the one used in the sp case (Eqs. (3)–(5)). The last two d orbitals correspond to Δ states, and the appropriate transformation is calculated using similar techniques. The wavefunctions including electron spin for the four Δ_{xy} states are

$$\begin{aligned}
|\Delta_{xy}\rangle|00\rangle &= \frac{1}{\sqrt{2}} [|^1\Delta_2\rangle - |^1\Delta_{-2}\rangle] \\
|\Delta_{xy}\rangle|1, -1\rangle &= \frac{1}{\sqrt{2}} [|^3\Delta_1\rangle - |^3\Delta_{-3}\rangle] \\
|\Delta_{xy}\rangle|10\rangle &= \frac{1}{\sqrt{2}} [|^3\Delta_2\rangle - |^3\Delta_{-2}\rangle] \\
|\Delta_{xy}\rangle|11\rangle &= \frac{1}{\sqrt{2}} [|^3\Delta_3\rangle - |^3\Delta_{-1}\rangle]. \quad (6)
\end{aligned}$$

The wavefunctions including electron spin for the four $\Delta_{x^2-y^2}$ states are

$$\begin{aligned}
|\Delta_{x^2-y^2}\rangle|00\rangle &= \frac{1}{\sqrt{2}} [|^1\Delta_2\rangle + |^1\Delta_{-2}\rangle] \\
|\Delta_{x^2-y^2}\rangle|1, -1\rangle &= \frac{1}{\sqrt{2}} [|^3\Delta_1\rangle + |^3\Delta_{-3}\rangle] \\
|\Delta_{x^2-y^2}\rangle|10\rangle &= \frac{1}{\sqrt{2}} [|^3\Delta_2\rangle + |^3\Delta_{-2}\rangle] \\
|\Delta_{x^2-y^2}\rangle|11\rangle &= \frac{1}{\sqrt{2}} [|^3\Delta_3\rangle + |^3\Delta_{-1}\rangle]. \quad (7)
\end{aligned}$$

Now that we have a relationship between the GAMESS basis and the basis needed for the sd case, we can write a 20×20 transformation matrix for electronic states. The transformation separates the states according to the Ω quantum number and facilitates the analysis of the results. There are ten distinct “spin-orbit constants” $A_1^{sd} - A_{10}^{sd}$ that define the possible matrix elements of \mathbf{H}_{so} between the molecular states in the sd case, and we relate them to the coupling between specific molecular states in Table 3. At large internuclear distance R , all the $A_1^{sd} - A_{10}^{sd}$ will approach 2/5 of the calculated spin-orbit splitting of the separated atom 2D state.

Table 3

Matrix elements of the spin-orbit Hamiltonian \mathbf{H}_{so} between the electronic states with the sd separated atom limit, for each value of Ω . At large R , $A_1^{sd} - A_{10}^{sd}$ all approach the atomic spin-orbit constant of the d atom.

Table 2

Matrix elements of the spin-orbit Hamiltonian \mathbf{H}_{so} between the electronic states correlating with the sp separated atom limit, for each value of Ω . At large R , $A_1^{sp} - A_5^{sp}$ all approach the atomic spin-orbit constant of the p atom.

$\Omega = \pm 2$		$^3\Pi$			
	$^3\Pi$	A_1^{sp}			
$\Omega = \pm 1$		$^1\Pi$	$^3\Pi$	$^3\Sigma^+$	
	$^1\Pi$	0	A_2^{sp}	A_3^{sp}	
	$^3\Pi$	A_2^{sp}	0	A_4^{sp}	
	$^3\Sigma^+$	A_3^{sp}	A_4^{sp}	0	
$\Omega = 0$		$^1\Sigma_0^+$	$^3\Pi_0$	$^3\Sigma_0^-$	$^3\Pi_0^-$
	$^1\Sigma_0^+$	0	$\sqrt{2}A_5^{sp}$	0	0
	$^3\Pi_0$	$\sqrt{2}A_5^{sp}$	$-A_1^{sp}$	0	0
	$^3\Sigma_0^-$	0	0	0	$\sqrt{2}A_4^{sp}$
	$^3\Pi_0^-$	0	0	$\sqrt{2}A_4^{sp}$	$-A_1^{sp}$

$\Omega = \pm 3$		$^3\Delta$			
	$^3\Delta$	A_1^{sd}			
$\Omega = \pm 2$		$^1\Delta$	$^3\Pi$	$^3\Delta$	
	$^1\Delta$	0	$A_2^{sd}/\sqrt{2}$	A_3^{sd}	
	$^3\Pi$	$A_2^{sd}/\sqrt{2}$	$A_4^{sd}/2$	$A_5^{sd}/\sqrt{2}$	
	$^3\Delta$	A_3^{sd}	$A_5^{sd}/\sqrt{2}$	0	
$\Omega = \pm 1$		$^1\Pi$	$^3\Delta$	$^3\Pi$	$^3\Sigma^+$
	$^1\Pi$	0	$A_6^{sd}/\sqrt{2}$	$A_7^{sd}/2$	$\sqrt{3}A_8^{sd}/2$
	$^3\Delta$	$A_6^{sd}/\sqrt{2}$	$-A_1^{sd}$	$A_5^{sd}/\sqrt{2}$	0
	$^3\Pi$	$A_7^{sd}/2$	$A_5^{sd}/\sqrt{2}$	0	$\sqrt{3}A_9^{sd}/2$
	$^3\Sigma^+$	$\sqrt{3}A_8^{sd}/2$	0	$\sqrt{3}A_9^{sd}/2$	0
$\Omega = 0$		$^1\Sigma_0^+$	$^3\Pi_0$	$^3\Sigma_0^-$	$^3\Pi_0^-$
	$^1\Sigma_0^+$	0	$\sqrt{3/2}A_{10}^{sd}$	0	0
	$^3\Pi_0$	$\sqrt{3/2}A_{10}^{sd}$	$-A_4^{sd}/2$	0	0
	$^3\Sigma_0^-$	0	0	0	$\sqrt{3/2}A_9^{sd}$
	$^3\Pi_0^-$	0	0	$\sqrt{3/2}A_9^{sd}$	$-A_4^{sd}/2$

3. Results and discussion

3.1. Comparison with other work

We first attempted to reproduce the results of Manaa [15] to validate our model. Manaa performed calculations of the spin-orbit matrix elements among the electronic states associated with the $3s4p$ limit ($1^1\Pi$, $1^3\Pi$, $2^1\Sigma^+$, and $2^3\Sigma^+$). His calculations used the full Breit–Pauli approximation, where both the spin-orbit and the spin-other-orbit contributions were included. His molecular orbitals were determined from a complete active-space multi-configuration self-consistent field (CAS-MCSCF) procedure. The CI included the single and double excitations of the electrons in the active space.

The present results for the spin-orbit matrix elements $A_1^{sp} - A_5^{sp}$ are compared with Manaa's results [15] in Fig. 2. The differences between these two calculations are typically on the order of 10–15%. For the asymptotic limit, our result is 14.3 cm^{-1} compared to Manaa's result of 14.9 cm^{-1} and the spectroscopic value of 19.2 cm^{-1} ($=1/3$ of 57.7 cm^{-1}). Both calculations underestimate the spectroscopic values by about 25%. We attribute the differences between the calculations primarily to Manaa's use of the two-electron expression for \mathbf{H}_{so} compared to the one-electron approximation we used [Eq. (1)]. Another possible source of the difference is that we used a larger basis set, since we wanted to study the behavior of higher excited states. The comparison between the present calculations and Manaa's results suggests that the uncertainties introduced by the small CI and the one-electron approximation for \mathbf{H}_{so} are not too large. We therefore have some confidence that our calculations will be useful for interpreting experimental results.

3.2. Spin-orbit matrix elements

Our calculations included all the molecular states approaching the following separated atom limits: $3s4s$, $3s4p$, $3p4s$, $3s5s$, $3s3d$,

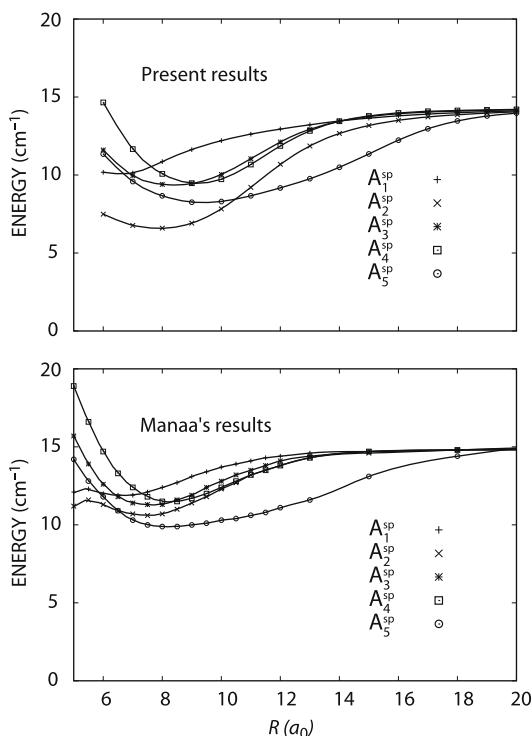


Fig. 2. Calculations of the spin-orbit coupling for the $3s4p$ case of NaK. The present results for $A_1^{sp} - A_5^{sp}$ are shown, as well as the previous calculations of Manaa [15]. Manaa's results for A_4^{sp} and A_5^{sp} were determined by dividing his reported $^3\Pi_0 - ^3\Sigma_0^+$ and $^3\Pi_0 - ^1\Sigma_0^+$ matrix elements by $\sqrt{2}$, according to Table 2.

$3s5p$, and $4s4s$. There are a total of 68 spin-orbit states, and we considered several R values in the range 6–100 a_0 . GAMESS calculated a 68×68 matrix at each R . Application of the models just described, which are based on 12 states correlating to an sp asymptote or 20 states correlating to the sd asymptote, posed some additional problems. The form of the electronic wavefunctions had to be carefully monitored as a function of R in order to identify the nature of each state. In many cases, an appropriate set of states could be isolated and treated separately. In other cases it was necessary to monitor curve crossings and switch the adiabatic states that were included in the analysis.

In the case of the $3s4p$ limit, it was easy to pick out the necessary states to include in the analysis since those electronic states did not have any large interactions with other electronic states. From Fig. 1 one can see that electronic states that go to $3p4s$, $3s5s$, $3s3d$, $3s5p$, and $4s4s$ limits will interact with each other at some values of internuclear distance R . In these cases it was necessary to include these interactions. GAMESS printed out a file with all the spin-orbit matrix elements (the 68×68 matrix). For each R , the electronic states for each 12 state sp model or for each 20 state sd model were identified. Our code read the entire matrix and then built a smaller matrix with just the appropriate matrix elements. These matrix elements were the spin-orbit couplings between electronic states as shown in Tables 2 and 3.

We treated several sets of potential curves separately. First, we obtained theoretical spin-orbit matrix elements for electronic states that go to the $3s3d$ limit. Fig. 3 shows that the calculated spin-orbit matrix elements $A_1^{sd} - A_{10}^{sd}$ for these electronic states approach the same asymptotic limit, as expected. More detailed figures and tables are available electronically [16]. Of these curves, A_4^{sd} was used to calculate the spin-orbit coupling constant A_v as a function of vibrational number for the $3^3\Pi$ electronic state.

The spin-orbit matrix elements $A_1^{sp} - A_5^{sp}$ for electronic states associated with the $3s5p$ limit are shown in Fig. 4, and tables are available electronically [16]. A_1^{sp} represents the spin-orbit coupling

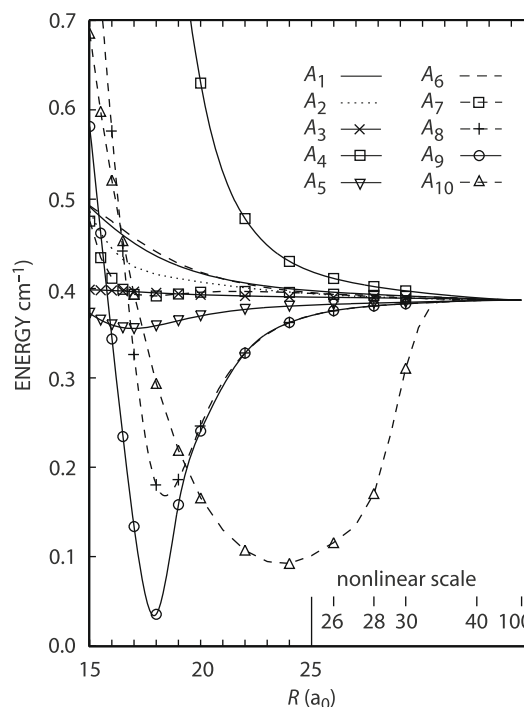


Fig. 3. Calculated spin-orbit coupling constants $A_1^{sd} - A_{10}^{sd}$ for the electronic states $5^{1,3}\Sigma^+$, $3^{1,3}\Pi$, and $1^{1,3}\Delta$ that correlate with the $3s3d$ limit. $A_9^{sd}/2$ is shown in more detail in Fig. 5. A_9^{sd} and A_{10}^{sd} appear anomalous due to an avoided crossing of an electronic state with the same Ω . The other state involved in this crossing dissociates to a different asymptotic limit.

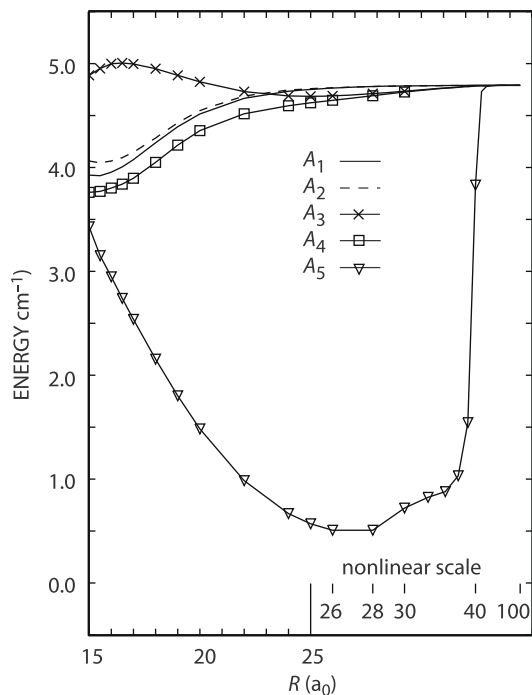


Fig. 4. Results for the electronic states $6^{1,3}\Sigma^+$ and $4^{1,3}\Pi$ that correlate with the $3s5p$ limit. The curves show the $A_1^{\text{sp}} - A_5^{\text{sp}}$ obtained in our calculation. The results for A_1^{sp} were used to calculate A_v for the $3^3\Pi$ state. A_5^{sd} appears anomalous due to an avoided crossing with an electronic state correlated with a different asymptotic limit.

of the $4^3\Pi$ state at $R > 15a_0$. A_1^{sp} is also needed to calculate the spin-orbit value as a function of vibrational number for the strongly interacting $3^3\Pi$ state.

3.3. Spin-orbit interaction of the $3^3\Pi$ and $4^3\Pi$ states

The results of the present theoretical calculations can be related to the experimental values of A_v for the $3^3\Pi$ state reported by Morgus et al. [4] if we obtain an expression for the spin-orbit interaction as a function of internuclear distance R . A_v is related to the internuclear separation by the following integral:

$$A_v = \frac{1}{2} \int |\chi_v(R)|^2 A_4^{\text{sd}}(R) dR, \quad (8)$$

where $\chi_v(R)$ is the vibrational wavefunction. We will include the factor of $\frac{1}{2}$ with $A_4^{\text{sd}}(R)$ when we discuss the spin-orbit interaction as a function of R .

The theoretical spin-orbit coupling terms $A_4^{\text{sd}}(R)/2$ for the $3^3\Pi$ and $A_1^{\text{sp}}(R)$ for the $4^3\Pi$ states are shown in Fig. 5(a). The sharp change between $R = 8$ and $9 a_0$ is due to the avoided crossing between these two electronic states (shown in bold in Fig. 1). To evaluate Eq. (8) we first determined the rovibrational wavefunctions for the $3^3\Pi$ state by using the theoretical curve obtained with the *ab initio* calculations. The vibrational wavefunctions were determined using LEVEL [17], which solves the radial Schrödinger equation for specific rovibrational levels.

Figure 6(a) shows the theoretical values of A_v calculated from Eq. (8) and the experimental values [4]. The structure in the calculated A_v near $v = 20$ may also be attributed to the avoided crossing of the $3^3\Pi$ adiabatic potential, which leads to a double well (see Fig. 1). For states with v in the range 15–25, some wavefunctions are localized in the inner well and others are in the outer well (examples of vibrational wavefunctions for several different levels of the $3^3\Pi$ double well potential were presented in Fig. 5 of Ref.

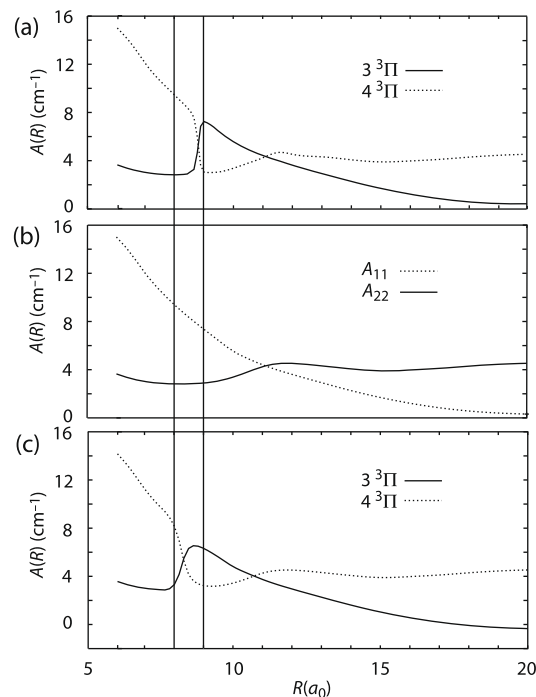


Fig. 5. Spin-orbit interaction as a function of R for the $3^3\Pi$ and the $4^3\Pi$ states. Panel (a) shows the results of *ab initio* calculations. The sharp change near $R = 8.8a_0$ is due to the avoided crossing of the $3^3\Pi$ and $4^3\Pi$ states. The curves corresponding to the $3^3\Pi$ and $4^3\Pi$ states are $A_4^{\text{sd}}/2$ and A_1^{sp} , respectively. Panel (b) shows effective spin-orbit coupling terms A_{11} and A_{22} that can be associated with diabatic curves that do not cross. Panel (c) shows modified $A_4^{\text{sd}}(R)/2$ and $A_1^{\text{sp}}(R)$ terms determined by using a more accurate form of the avoided crossing, as described in the text.

[4]). $A_4^{\text{sd}}(R)/2$ is different for these two regions of R ; the switch between inner well and outer well values causes the sharp structure in the solid curve in Fig. 5(a). The values of A_v obtained by the convolution in Eq. (8) therefore vary sharply depending on the details of the vibrational wavefunctions.

The foregoing discussion leads to the conclusion that reliable potential curves are critical for the calculation of accurate A_v . The

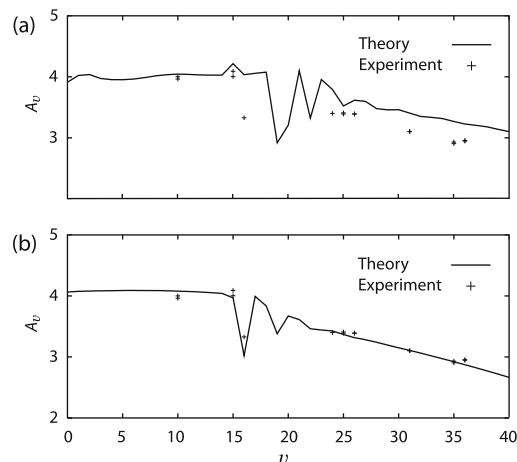


Fig. 6. Calculated values of the spin-orbit constant A_v for the $3^3\Pi$ state are compared with the measurements of Morgus et al. [4]. Panel (a) shows values calculated using vibrational wavefunctions determined from the present *ab initio* potential curve. Panel (b) shows corresponding results using vibrational wavefunctions determined from the fitted potential curves of Miles et al. [6]. In both cases, the theoretical spin-orbit interaction from the present work was used. At $v = 16$ and 19, the values of A_v are lower due to these rovibrational levels being mostly in the inner well of the $3^3\Pi$ state.

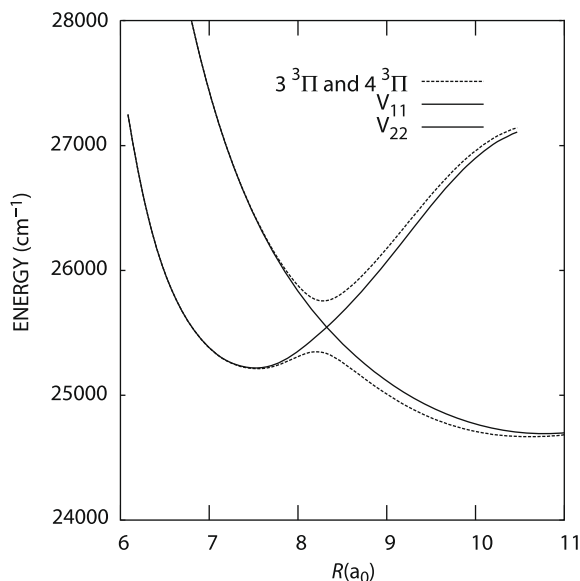


Fig. 7. Diabatic (—) and adiabatic (---) potential curves for the coupled $3^3\Pi$ and $4^3\Pi$ states determined by Miles et al. [6].

location of the sharp structure in A_4^{sd} and the form of the vibrational wavefunctions in the double well potential are both sensitive to the details of the avoided crossing of the $3^3\Pi$ and $4^3\Pi$ states. The results presented in Fig. 6(a) were calculated using vibrational wavefunctions determined from our *ab initio* potentials, which are less precise than those determined by fitting high resolution spectroscopic data. Fortunately, previous work in our group has led to the determination of precise $3^3\Pi$ and $4^3\Pi$ potential curves and the coupling between them [4,6]. Miles et al. [6] determined accurate diabatic potential curves and coupling terms for these states by fitting the experimental data. We have performed additional calculations using these more accurate curves.

The adiabatic and diabatic potential curves determined by Miles et al. [6] are shown in Fig. 7. For these curves the avoided crossing occurs at a slightly smaller value of R than we obtained in our *ab initio* calculations, and it is necessary to modify the form of $A_4^{sd}(R)/2$ to account for this difference. The results for $A_4^{sd}(R)/2$ for the $3^3\Pi$ and $A_1^{sp}(R)$ for the $4^3\Pi$ states shown in Fig. 5(a) may be considered “adiabatic” functions. By interpolating between values of $A_4^{sd}(R)/2$ and $A_1^{sp}(R)$ away from the point of maximum coupling, we were able to estimate corresponding “diabatic” functions that can be associated with the diabatic potentials determined by Miles et al. [6]. Then we used the coupling terms of Miles et al. to calculate improved values of the spin–orbit coupling for each of the adiabatic states. The adiabatic coupling terms are weighted averages of the diabatic functions shown in Fig. 5(b), where the weights are determined from the work of Miles et al. [6]. This procedure leads to the adjusted $A_4^{sd}(R)/2$ and $A_1^{sp}(R)$ shown in Fig. 5(c). Using the modified form of $A_4^{sd}(R)/2$ (the solid line in Fig. 5(c)), and using Miles’ adiabatic potential to determine the vibrational wavefunctions, we recalculated the A_ν for the $3^3\Pi$ state. The results, which are shown in Fig. 6(b), compare very well with the known experimental values of the $3^3\Pi$ state.

Corresponding calculations were also performed for the $4^3\Pi$ state. We used the upper adiabatic potential determined by diagonalizing Miles’ diabatic potential matrix [6] at each R and calculated vibrational wavefunctions using LEVEL [17]. The resulting A_ν , which are tabulated in Table 4, do not exhibit the dramatic fluctuations found for the $3^3\Pi$. This result is easily understood. The $4^3\Pi$ states considered are all localized in the same range of R , and the A_ν obtained correspond closely to the average value of

Table 4

Values of A_ν for $4^3\Pi$ rovibrational levels calculated by convoluting the spin–orbit coupling function $A_1^{sp}(R)$ with the appropriate vibrational wavefunction $\chi_{v,j}(R)$.

ν	$J = 14$	$J = 30$	$J = 45$
0	5.78 cm^{-1}	5.75 cm^{-1}	5.70 cm^{-1}
1	5.75	5.72	5.67
2	5.74	5.71	5.66
3	5.74	5.71	5.66
4	5.72	5.69	5.65
5	5.70	5.67	5.63
6	5.67	5.64	5.60

$A_1^{sp}(R)$ in that range. At this point, we cannot make a comparison with experimental data. Although some preliminary data are available [11], a full deperturbation analysis has not yet been performed.

4. Concluding remarks

We have calculated spin–orbit coupling terms as a function of R for selected excited states of NaK. Convolution of these coupling terms with appropriate vibrational wavefunctions provides spectroscopic constants that can be compared with recent experimental studies. Our results provide a quantitative model for the strong dependence on vibrational quantum number ν of the spin–orbit coupling constant A_ν for the double well $3^3\Pi$ state. We emphasize, however, the importance of using very accurate potentials and vibrational wavefunctions in the calculation.

Acknowledgment

This work was supported by the National Science Foundation Grant No. PHY-0652938.

Appendix A. Supplementary data

Supplementary data associated with this article can be found, in the online version, at doi:10.1016/j.jms.2009.08.012. Supplementary data for this article are available on ScienceDirect (www.sciencedirect.com) and as part of the Ohio State University Molecular Spectroscopy Archives (http://library.osu.edu/sites/msa/jmsa_hp.htm).

References

- [1] J. Huennekens, I. Prodan, A. Marks, L. Sibbach, E. Galle, T. Morgus, Li Li, Experimental studies of the NaK $1^3\Delta$ state, *J. Chem. Phys.* 113 (2000) 7384–7397.
- [2] P. Burns, L. Sibbach-Morgus, A.D. Wilkins, F. Halpern, L. Clarke, R.D. Miles, Li Li, A.P. Hickman, J. Huennekens, The $4^2\Sigma^+$ state of NaK: potential energy curve and hyperfine structure, *J. Chem. Phys.* 119 (2003) 4743–4754.
- [3] P. Burns, A.D. Wilkins, A.P. Hickman, J. Huennekens, The NaK $1(b)^3\Pi_{\Omega=0}$ state hyperfine structure and the $1(b)^3\Pi_{\Omega=0} \sim 2(A)^1\Sigma^+$ spin–orbit interaction, *J. Chem. Phys.* 122 (2005) 074306.
- [4] L. Morgus, P. Burns, R.D. Miles, A.D. Wilkins, U. Ogba, A.P. Hickman, J. Huennekens, Experimental study of the NaK $3^3\Pi$ double minimum state, *J. Chem. Phys.* 122 (2005) 144313.
- [5] A.D. Wilkins, L. Morgus, J. Hernandez-Guzman, J. Huennekens, A.P. Hickman, The NaK $1^3\Delta$ states: Theoretical and experimental studies of fine and hyperfine structure of ro-vibrational levels near the dissociation limit, *J. Chem. Phys.* 123 (2005) 124306.
- [6] R.D. Miles, L. Morgus, D.O. Kashinski, J. Huennekens, A.P. Hickman, Nonadiabatic coupling in the $3^3\Pi$ and $4^3\Pi$ states of NaK, *J. Chem. Phys.* 125 (2006) 154304.
- [7] H. Sun, J. Huennekens, Spin-orbit perturbations between the $A(2)^1\Sigma^+$ and $b(1)^3\Pi_0$ states of NaK, *J. Chem. Phys.* 97 (1992) 4714–4722.
- [8] E.A. Pazyuk, A.V. Stoliarov, A. Zaitsevskii, R. Ferber, P. Kowalczyk, C. Teichtel, Spin–orbit coupling in the $D^1\Pi \sim d^3\Pi$ complex of $^{23}\text{Na}^{39}\text{K}$, *Mol. Phys.* 96 (1999) 955–961.

- [9] S. Eckel, S. Ashman, J. Huennekens, Spin-orbit coupling of the NaK $3^3\Pi$ and $3^1\Pi$ states: determination of the coupling constant and observation of quantum interference effects, *J. Mol. Spectrosc.* 242 (2007) 182–194.
- [10] M.W. Schmidt, K.K. Baldrige, J.A. Boatz, S.T. Elbert, M.S. Gordon, J.H. Jensen, S. Koseki, N. Matsunaga, K.A. Nguyen, S. Su, T.L. Windus, M. Dupuis, J.A. Montgomery Jr., General atomic and molecular electronic structure system, *J. Comp. Chem.* 14 (1993) 1347–1363.
- [11] L. Morgus, Perturbation-facilitated optical-optical double resonance studies of the $3^3\Pi$ and $4^3\Pi$ states of NaK, Ph.D. thesis, Lehigh University, unpublished (2005).
- [12] S. Magnier, M. Aubert-Frécon, Ph. Millié, Potential energies, permanent and transition dipole moments for numerous electronic excited states of NaK, *J. Mol. Spectrosc.* 200 (2000) 96–103.
- [13] T.H. Dunham, Gaussian basis functions for use in molecular calculations. iii. contraction of (10s6p) atomic basis sets for the first row atoms, *J. Chem. Phys.* 55 (1971) 716–723.
- [14] H. Lefebvre-Brion, R.W. Field, *The Spectra and Dynamics of Diatomic Molecules*, Elsevier Inc., San Diego, CA, 2004.
- [15] M.R. Manaa, Photodissociation of NaK: *ab initio* spin-orbit interactions of the Na(3^2S) K(4^3P_j) manifold, *Int. J. Quant. Chem.* 75 (1999) 693–697.
- [16] Supplementary Material, included as supplementary data on Science Direct, 2009, as described in Appendix A.
- [17] R.J. Le Roy, LEVEL 8.0: A computer program for solving the radial Schrödinger equation for bound and quasibound levels, Chemical Physics Research Report No. CP-663, University of Waterloo, 2007. <http://leroy.uwaterloo.ca/programs.html>.